Driven flow with exclusion and spin-dependent transport in graphenelike structures

S. L. A. de Queiroz*
Instituto de Física, Universidade Federal do Rio de Janeiro, Caixa Postal 68528, 21941-972 Rio de Janeiro RJ, Brazil

R. B. Stinchcombe†
Rudolf Peierls Centre for Theoretical Physics, University of Oxford, 1 Keble Road, Oxford OX1 3NP, United Kingdom

(Dated: April 14, 2017)

We present a simplified description for spin-dependent electronic transport in honeycomb-lattice structures with spin-orbit interactions, using generalizations of the stochastic non-equilibrium model known as the totally asymmetric simple exclusion process. Mean field theory and numerical simulations are used to study currents, density profiles and current polarization in quasi- one dimensional systems with open boundaries, and externally-imposed particle injection (α) and ejection (β) rates. We investigate the influence of allowing for double site occupancy, according to Pauli's exclusion principle, on the behavior of the quantities of interest. We find that double occupancy shows strong signatures for specific combinations of rates, namely high α and low β, but otherwise its effects are quantitatively suppressed. Comments are made on the possible relevance of the present results to experiments on suitably doped graphenelike structures.

arXiv:1702.04553v2 [cond-mat.stat-mech] 13 Apr 2017

I. INTRODUCTION

In this paper we consider a simplified model for spin-dependent electronic transport in honeycomb-lattice structures with spin-orbit (SO) interactions. Suitable generalizations of the totally asymmetric simple exclusion process (TASEP) are applied to such systems. This extends previous work which dealt with steady-state properties [1] and dynamics [2] of the most basic implementation of the TASEP on honeycomb-lattice geometries.

The TASEP, in its one-dimensional (1D) version, already exhibits many non-trivial properties because of its collective character [3–9]. It has been used, often with adaptations, to model a broad range of non-equilibrium physical phenomena, from the macroscopic level such as highway traffic [10] to the microscopic, including sequence alignment in computational biology [11] and current shot noise in quantum-dot chains [12].

In the time evolution of the 1D TASEP, the particle number n_ℓ at lattice site ℓ can be 0 or 1, and the forward hopping of particles is only to an empty adjacent site. In addition to the stochastic character provided by random selection of site occupation update [13, 14], the instantaneous current $\hat{J}_{\ell\,\ell+1}$ across the bond from ℓ to $\ell+1$ depends also on the stochastic attempt rate, or bond (transmissivity) rate, t_ℓ, associated with it. Thus,

$$\hat{J}_{\ell\,\ell+1} = \begin{cases} n_\ell(1-n_{\ell+1}) & \text{with probability } t_\ell \\ 0 & \text{with probability } 1-t_\ell \ . \end{cases} \tag{1}$$

In Ref. 12 it was argued that the ingredients of 1D TASEP are expected to be physically present in the description of electronic transport on a quantum-dot chain; namely, the directional bias would be provided by an external voltage difference imposed at the ends of the system, and the exclusion effect by on-site Coulomb blockade. Following similar lines, the present work with its emphasis on honeycomb structures is partly motivated by recent progress in the physics of graphene and its quasi-1D realizations, such as nanotubes and nanoribbons [15–17]. Being a classical model, the TASEP does not incorporate quantum interference effects which play an important role in electronic transport. However, when considering transport in carbon allotropes under an applied bias the lattice topology affects how currents combine, and how they are microscopically located, whether classical or quantum. These features show up in the model we treat by such effects as the sublattice structure seen in steady-state currents and densities for the hexagonal lattice [1, 2].

Here we focus on modeling the behavior of spin polarization [18] in graphene-like quasi–1D geometries, in the presence of SO couplings [19]. The spin-flipping character of SO interactions is represented, e.g., in a tight-binding description, by a non-diagonal 2×2 matrix in the space of eigenfunctions of the electron's spin σ_z [20–25]. Although the effective strength of intrinsic SO coupling in graphene is estimated to be $25-50\ \mu$eV [26], much smaller than the nearest-neighbor hopping $\gamma_0 = 2.8$ eV [15], doping with suitable impurities can result in samples where SO interactions are more significant in specific neighborhoods next to impurity locations [27–30].

In Sec. II we briefly recall basic features of the spin-independent TASEP model used in Refs. 1 and 2, and outline the adaptations and approximations here added to the model, in order to describe spin polarization, SO interactions, and spin-dependent currents. A mean field

* sldq@if.ufrj.br
† Robin.Stinchcombe@physics.ox.ac.uk

theoretical description is given for the problem. The corresponding numerical tests are given in Sec. III. Section IV is devoted to discussions and conclusions.

II. TASEP MODEL: THEORY

A. Introduction

We only consider cases where mean flow direction is parallel to one of the lattice directions, and bond rates are independent of coordinate transverse to the flow direction. These configurations have no bonds orthogonal to the mean flow direction; thus they fall easily within the generalized TASEP description to be used, where each bond is to have a definite directionality, compatible with that of average flow. Furthermore, for simplicity we always use periodic boundary conditions (PBC) across. So, in the terminology of quasi 1D carbon nanotubes (CNT) and nanoribbons (CNR) [15], the structures to be discussed correspond to zigzag CNTs. Most experimental studies, as well as many theoretical ones, deal with impurities on CNRs. However, edge effects play an important role in the energetics of favored defect locations for the latter type of system. Since here we shall not attempt detailed numerical comparisons to experimental data, our choice of considering only nanotube geometries where we need not account for this sort of positional preference inhomogeneity, is justified on grounds of keeping the number of relevant parameters to a minimum.

The structures studied here have an integer number of elementary cells (one bond preceding a full hexagon) along the mean flow direction, see Refs. 1 and 2. Also, we have to expect a two-sublattice character in general [1].

Open boundary conditions are used at both ends of the strip with the associated, externally imposed, injection and ejection (attempt) rates α and β [3, 6]. For all internal bonds ℓ we take their transmissivity rates, defined in Eq. (1), to be $t_\ell \equiv 1$.

Thus a nanotube with N_r elementary cells parallel to the flow direction, and N_w transversally, has $N_s = N_w \times (4N_r+1)$ sites and $N_b = N_w \times (6N_r+2)$ bonds (including the injection and ejection ones).

In the TASEP context, the simplest way to simulate the effects associated with SO couplings in doped systems is by assigning a quenched random distribution of *spin-flipping sites* (substitutional impurities) to an otherwise pure sample, with the following rule: every time a particle passes through such a site the z component of its spin 1/2 will change sign, with probability π_f (or remain the same, with probability $1-\pi_f$). In what follows, we shall always take $\pi_f = 1$ for simplicity. All the original TASEP rules are kept except that, regarding exclusion effects, the physical properties of the problem under investigation immediately suggest two plausible alternatives:
(A) Keep the maximum occupation per site $n_\ell = 1$ as in the original formulation, or
(B) Allow two particles simultaneously on the same site, provided that their spins are opposite (thus mimicking Pauli's principle).

In model (A), polarization and global current (and density) aspects are decoupled. Thus, although the evolution of spin polarization along the system shows interesting and nontrivial features, overall currents and total (spin-up plus spin-down) density profiles will be the same as in the spinless cases studied in Refs. 1 and 2. On the other hand, we will see that model (B) exhibits some rather intricate interplay between spin and real-space degrees of freedom.

B. Mean field description

1. *Impurity-induced spin polarization decay*

Initially we give a simplified approach to describe the behavior of spin polarization, by focusing on the path followed by a single particle traveling along the system, in the course of which spin-flipping events may occur. With $x_i \ll 1$ being the concentration of spin-flipping (impurity) sites, the TASEP directionality rules imply that, for a system with N_r rings along the flow direction, each particle flowing through the nanostructure will have to go through exactly $N = 4N_r + 1$ sites. Assume impurities to be uniformly distributed along the system according to a grand-canonical distribution with mean x_i; replace each slice of the nanotube across the average flow direction with an "effective" site (N in all); and take x_i as the probability of stepping on an impurity at each "effective" site. So we are replacing the actual realizations of random discrete spin-flipping sites by a homogeneous "effective medium" with a probability per slice x_i of the particle's spin being flipped. Recalling that the particle's spin upon exiting at the ejection point will depend only on whether it has met an even or odd number of impurities, elementary probabilistic considerations allow one to work out the exact probability distribution for the current polarization at any cross section (take, for simplicity, a fully-polarized injected current). The spin fraction of the average exiting current with plus or minus spin turns out to be, for $N \gg 1$,

$$P_\pm = \frac{1}{2}\left[1 \pm (1-2x_i)^N\right] \ , \tag{2}$$

whence the (ensemble-averaged) exit polarization is

$$\langle \mathcal{P}(x_i) \rangle \propto \exp(-N/N_0) \ , \quad N_0 = -[\ln(1-2x_i)]^{-1} \ . \tag{3}$$

Such an effective-medium approach of course neglects all correlations between particle occupation at neighboring sites and the corresponding local currents, recall Eq. (1); its predictions are also independent of whether model (A) or (B) is adopted. Furthermore, the results for normalized polarizations will depend only on x_i and on the position ℓ ($1 \le \ell \le 4N_r + 1$) of the cross-section under

consideration, and *not*, e.g., on the value of the (α- and β- dependent) steady-state current through the system. In Sec. III we test the predictions of this simplified description against the results of numerical simulations.

2. Currents and density profiles

The mean field description of total currents and density profiles in model (A) is identical to that for spinless models, and is given at length in Refs. 1 and 2.

In model (B) there are four mutually exclusive possibilites for occupation of a site: vacant, one particle with plus spin, one particle with negative spin, and two particles with opposite spins. Their associated probabilities for site ℓ are denoted respectively by p^0_ℓ, p^+_ℓ, p^-_ℓ, p^{+-}_ℓ, with $p^0_\ell + p^+_\ell + p^-_\ell + p^{+-}_\ell = 1$.

We also use here corresponding state indicator variables $\hat{p}^0_\ell$, $\hat{p}^+_\ell$, $\hat{p}^-_\ell$, $\hat{p}^{+-}_\ell$, such that, for example, $\hat{p}^+_\ell$ can be one or zero, respectively specifying that site ℓ is occupied or not by a spin + particle. Then p^+_ℓ is the average of $\hat{p}^+_\ell$; and so on .

Ignoring, until stated otherwise, the possible effect of impurities, the possible updates of bonds linking, say, sites ℓ and $\ell+1$ contributing to the instantaneous plus-spin current $\hat{J}^+$ through transfer across of a + spin particle have initial configurations with the following indicators: $\hat{p}^+_\ell \hat{p}^0_{\ell+1}$, $\hat{p}^+_\ell \hat{p}^-_{\ell+1}$, $\hat{p}^{+-}_\ell \hat{p}^-_{\ell+1}$, $\hat{p}^{+-}_\ell \hat{p}^0_{\ell+1}$.

Those for $\hat{J}^-$ have a similar set but with + and − superscripts interchanged.

From the bond update details given at the beginning of Sec. III, unit bond rates are associated with the first three configurations listed for each of $\hat{J}^+$ and $\hat{J}^-$, while the rate is $\frac{1}{2}$ for the last (shared) configuration. Consequently, in place of Eq. (1), for any configuration of the system with model (B) the currents on bond ℓ, $\ell+1$ are given (exactly) in terms of the indicator variables [collectively denoted as $\{\hat{p}\}$] by:

$$\begin{aligned}\hat{J}^+_{\ell\,\ell+1} &= \hat{p}^+_\ell \hat{p}^0_{\ell+1} + \frac{1}{2}\hat{p}^{+-}_\ell \hat{p}^0_{\ell+1} + \hat{p}^+_\ell \hat{p}^-_{\ell+1} + \hat{p}^{+-}_\ell \hat{p}^-_{\ell+1} \\ &\equiv C^+_{\ell\,\ell+1}(\{\hat{p}\}) \; ; \end{aligned} \tag{4}$$

$$\begin{aligned}\hat{J}^-_{\ell\,\ell+1} &= \hat{p}^-_\ell \hat{p}^0_{\ell+1} + \frac{1}{2}\hat{p}^{+-}_\ell \hat{p}^0_{\ell+1} + \hat{p}^-_\ell \hat{p}^+_{\ell+1} + \hat{p}^{+-}_\ell \hat{p}^+_{\ell+1} \\ &\equiv C^-_{\ell\,\ell+1}(\{\hat{p}\}) \; . \end{aligned} \tag{5}$$

The currents $\hat{J}^+_{\ell\,\ell+1}$, $\hat{J}^-_{\ell\,\ell+1}$ have no terms with factors $\hat{p}^0_\ell$ or $\hat{p}^{+-}_{\ell+1}$, for obvious physical reasons. With $\hat{I}$ denoting the identity indicator, that means that they can, for example, be multiplied by $(\hat{I} - \hat{p}^{+-}_{\ell+1})$, to give new forms $\hat{J}^\pm_{\ell\,\ell+1} = C^{\pm\,\prime}_{\ell\,\ell+1} = C^\pm_{\ell\,\ell+1}(\hat{I} - \hat{p}^{+-}_{\ell+1})$ which are still exact.

The most direct and obvious mean field approximation for the mean currents J^+, J^- is obtained by replacing each $\hat{p}$ in the C^+, C^- of Eqs. (4)– (5) by its average p. The resulting form proves to be entirely adequate for most purposes in this investigation. But equally well one could have made the mean field replacement using the equivalent forms $C^{+\,\prime}$, $C^{-\,\prime}$, which results in a different mean field description.

The latter description is slightly more complicated but it might be expected to better capture the physics of the process in the high density regions, where large $p^{+-}_{\ell+1}$ suppresses the current. So it will be used in Sec. III C for one such case. Apart from there we use mean field approximations with mean currents $J^\pm_{\ell\,\ell+1} = C^\pm_{\ell\,\ell+1}(\{p\})$.

The original mean field theory for the TASEP chain assumes approximate factorization of correlation functions. In the same spirit we will approximate p^{+-}_ℓ by $p^+_\ell\, p^-_\ell$. It will be seen that this gives completeness to the set of steady state mean field equations that arises from conservation of the + and − spin currents J^+, J^-, at each vertex including boundary vertices $\ell = 0$, L in the case of open boundary conditions. With this approximation, the mean number of + (R_ℓ) or − (S_ℓ) spin particles at site ℓ are respectively:

$$R_\ell = p^+_\ell(1 + p^-_\ell) \quad ; \quad S_\ell = p^-_\ell(1 + p^+_\ell) \; . \tag{6}$$

Then, using also $p^0_\ell + p^+_\ell + p^-_\ell + p^{+-}_\ell = 1$, the mean field equations for the average currents become

$$\begin{aligned}J^+_{\ell\,\ell+1} &= \hat{p}^+_\ell \left(1 + \frac{1}{2}p^-_\ell\right)\left[1 - (p^+_{\ell+1} + p^-_{\ell+1} + p^+_{\ell+1}p^-_{\ell+1})\right] \\ &\quad + p^+_\ell(1 + p^-_\ell)p^-_{\ell+1} \equiv f(p^+_\ell, p^-_\ell, p^+_{\ell+1}, p^-_{\ell+1}) \; ; \end{aligned} \tag{7}$$

$$\begin{aligned}J^-_{\ell\,\ell+1} &= p^-_\ell \left(1 + \frac{1}{2}p^+_\ell\right)\left[1 - (p^+_{\ell+1} + p^-_{\ell+1} + p^+_{\ell+1}p^-_{\ell+1})\right] \\ &\quad + p^-_\ell(1 + p^+_\ell)p^+_{\ell+1} \equiv f(p^-_\ell, p^+_\ell, p^-_{\ell+1}, p^+_{\ell+1}) \; . \end{aligned} \tag{8}$$

Similarly, with + spin particles injected at rate α^+ at the left boundary site $\ell = 0$ the mean current J^+ entering there is

$$J^+_0 = \alpha^+\left[1 - p^+_0(1 + p^-_0)\right] \; . \tag{9}$$

Likewise, with ejection rate β^+ for + spin particles at the right boundary site $\ell = L$, the mean current J^+ leaving there is

$$J^+_L = \beta^+ p^+_L(1 + p^-_L) \; . \tag{10}$$

The corresponding boundary currents for − spin particles satisfy corresponding equations in which the + and − signs are interchanged.

The study of steady state properties involves relating the currents J^+, J^- and the density profiles R_ℓ, S_ℓ to the injection and ejection rates α^+, α^-, β^+, β^-. In general this involves the use of profile maps resulting from current conservation at each lattice vertex.

3. Model (B) on linear chain (without impurities)

As will be seen below, for model (B) on the nanotube the maps are quite complex, being two-stage maps of four

sets of variables (p_ℓ^+ and p_ℓ^- for two sublattices), so we first go to the simpler and more transparent case of model (B) on the linear chain, still without impurities.

There, in the steady state all bonds ℓ, $\ell+1$ carry the same J^+ and the same J^-, which must also equal the injected and ejected currents. For $0 \le \ell \le L-1$, using Eqs. (7) and (8),

$$f(p_\ell^+, p_\ell^-, p_{\ell+1}^+, p_{\ell+1}^-) = J_0^+ = J_L^+ \ ; \tag{11}$$

$$f(p_\ell^-, p_\ell^+, p_{\ell+1}^-, p_{\ell+1}^+) = J_0^- = J_L^- \ , \tag{12}$$

where J_0^+, J_L^+ are given in Eqs. (9) and (10) (similarly for J_0^-, J_L^-).

Eqs. (11), (12) constitute the "one-stage" map giving, in principle, for specified currents, $p_{\ell+1}^+$ and $p_{\ell+1}^-$ in terms of p_ℓ^+ and p_ℓ^- and finally, using the detailed forms of the injection and ejection currents, all p_ℓ^+, p_ℓ^- and currents in terms of the boundary rates. This description properly handles, through the specific forms of current in Eqs. (7), (8) the new effects of the conditional double occupancy in model (B). Furthermore, the description is clearly complete (with the use of the approximation $p^{+-} = p^+ p^-$).

By exploiting the symmetries and relative simplicity of the dependences on p_ℓ^+, p_ℓ^-, $p_{\ell+1}^+$, $p_{\ell+1}^-$ of the combinations $J_{\ell\,\ell+1}^+ \pm J_{\ell\,\ell+1}^-$ it is possible to obtain explicit functional forms for $p_{\ell+1}^+$, $p_{\ell+1}^-$ in terms of p_ℓ^+, p_ℓ^-, and the constant values of J^+, J^-:

$$p_{\ell+1}^+ = \frac{1}{2A}\left[-(B+CA) \pm \sqrt{(B+CA)^2 - 4A(Cp_\ell^- - D)}\right] \tag{13}$$

$$p_{\ell+1}^- = p_{\ell+1}^+ + C \ , \tag{14}$$

where

$$A = p_\ell^+ + p_\ell^- + p_\ell^+ p_\ell^- \ ; \ B = p_\ell^+ + p_\ell^- \ ;$$
$$D = A - (J^+ + J^-) \ ; \ C = \frac{J^+ - J^-}{p_\ell^+ p_\ell^-} \ . \tag{15}$$

This gives the explicit two-variable profile map for model (B) on the linear chain.

We next consider the possible fixed points of the map. There can be two real (physical) ones, at $(p_\ell^+, p_\ell^-) = (p_<^+, p_<^-)$ and $(p_>^+, p_>^-)$, the first ("lower") one having entries lower than those in the other ("upper") one, and they correspond to unstable (repulsive) and stable (attractive) ones, respectively, in the forward mapping $\ell \to \ell+1$.

So, e.g., starting with p^+ and p^- between the fixed points and very close to the lower one, at first many iteration steps leave (p^+, p^-) close to the starting value before it rapidly moves away and homes in on the attractive fixed point. So the associated profile (p_ℓ^+, p_ℓ^-) has p_ℓ^+ and p_ℓ^- both monotonically increasing with ℓ and each qualitatively similar to the low-current-phase form $a + b\tanh(\phi + \ell\theta)$ of the mean field TASEP chain, with $a - b = p_<$, $a + b = p_>$ for each of p_ℓ^+ and p_ℓ^-.

For the other possibilities (two coincident physical fixed points or none) the possible profiles are again qualitatively similar to those of the TASEP at its critical point or in its maximal current phase (i.e., with $-\tan$ replacing tanh). So for model (B) on the chain without impurities the mean field phase diagram and density profiles in the various phases are like those of the TASEP chain.

For a quantitative example we proceed next from the full formalism of Eqs. (13)–(15) to the case with boundary conditions, such that the map has a fixed point at $p_\ell^+ = p_\ell^- \equiv x^*$, corresponding to equal and level density profiles for spin up and spin down particles (hence, unpolarized). From the results above, this is only possible if

$$J^+ = J^- = x^* - \frac{1}{2}x^{*2} - x^{*3} - \frac{1}{2}x^{*4} \ . \tag{16}$$

The level profiles will normally extend to one or the other boundary, depending on the relative sizes of the injection and ejection rates. Then we may use the relationship of J^+, J^- to the rates at that boundary. For example, when that boundary is the injection site the above analysis shows that for equal level profiles $\alpha^+ = \alpha^-$ is needed, and then

$$J^+ = J^- = \alpha\left[1 - x^*(1+x^*)\right] \ . \tag{17}$$

The corresponding level spin up and spin down particle densities are then

$$R = S = x^*(1+x^*) \ , \tag{18}$$

with no net polarization.

Eq. (16) also allows the extraction of the maximal current J_m for level profiles, and shows that it occurs when the two fixed points become coincident. This is because the function on the right hand side of Eq. (16) has a single maximum in the physical region $x^* \ge 0$. It is then the $J^+ = J^-$ value at which the two solutions (fixed points) come together. One gets $J_m^+ = J_m^- = 0.243207\ldots$ for $x_m^* = 0.39817\ldots$, so $R_m = S_m = 0.55671\ldots$. These predictions are compared to simulational results in Sec. III B below.

Finally, concerning model (B) on the pure chain we note that with fully polarized injection, e.g., $\alpha^+ = 1$, $\alpha^- = 0$ no double occupancy occurs at any site, so all properties become identical to those of the standard TASEP.

4. Model (B) on nanotube (without impurities)

As in previous studies [1, 2], what follows for model (B) on the nanotube concerns situations with azimuthal symmetry. The "top" open boundary of the hexagonal nanotube is taken to be the ring of sites all with $\ell = 0$, all

having the same injection rates (α^+, α^-); similarly with the ejection sites, at $\ell = L$ at the other end of the tube. So ℓ indicates site position down the tube and no site azimuth coordinate will be needed for the steady state properties here discussed.

For the TASEP on the nanotube it is necessary to distinguish two sublattices, "even" and "odd". At each interior site of the even sublattice (having even label) two bonds are incident from above and one leaves below, and vice versa for all odd sublattice sites; for a pictorial representation see Fig. 1 of Ref. 2. We take L even ($L = 2M$) so that injection and ejection are on the same (even) sublattice.

Because of the branching and recombination of bonds referred to above, in the steady state each bond $(2\ell, 2\ell+1)$ (for all ℓ) carries the same (J^+, J^-) which is twice that for each bond $(2\ell+1, 2\ell+2)$ (all ℓ) and the same as the injection (J_0^+, J_0^-) and ejection (J_L^+, J_L^-). That is, for $\sigma = \pm$,

$$J^\sigma_{2\ell\, 2\ell+1} = 2J^\sigma_{2\ell+1\, 2\ell+2} = J_0^\sigma = J_L^\sigma \ , \qquad (19)$$

for any ℓ in $[0, M-1]$.

The J^σ's here are as given in terms of $\{p_\ell^+, p_\ell^-\}$ by Eqs. (7)–(10). The current-balance Eqs. (19) above provide the mapping relationships between probability variables at successive positions ℓ, in principle enough to find all mean field profiles and currents in terms of boundary rates. But successive sites lie on different sublattices so, as in previous studies [1, 2] any, even qualitative, connection with analytic functions requires a two-stage map between adjacent sites on the same sublattice, via one on the other sublattice. The quadratic dependence of bond currents on p variables of both sites they link, coming from the conditional double occupancy, is a further complicating feature, making most further progress purely numerical.

Nevertheless more analytic progress is possible concerning the fixed points of the two-stage mapping for a given sublattice, whose connection with level portions of particle density profiles associated with low current phases, and with maximal current aspects have been exploited in Sec. II B 3 above. We next consider these, using the example of unpolarized cases.

For fully unpolarized systems, e.g., arising from $\alpha^+ = \alpha^- = \alpha$, $\beta^+ = \beta^- = \beta$, we have $p_\ell^+ = p_\ell^- \equiv p_\ell$, and $J^+ = J^-$ on each sublattice. The fixed points of the two-step map then correspond to having all p_ℓ the same on each sublattice, i.e.,

$$p_{2\ell} = u \ , \quad p_{2\ell+1} = v \qquad (\text{all } \ell) \ , \qquad (20)$$

with u and v the level values of the probabilities at the sites of the two sublattices.

Then, from Eq. (19) the two-stage map from a site on the even sublattice to a forward adjacent site (on the odd sublattice), and then from there to a further forward adjacent site on the even sublattice is

$$f(u,u,v,v) = J_0 = J_L \ ; \qquad f(v,v,u,u) = \frac{1}{2} J_0 \ . \quad (21)$$

Numerical methods can readily provide solutions of these equations for u, v for a range of specified values of J_0, from zero to a cutoff at $J_0 \approx 0.332$. For small J_0, the behavior of u and v is given by

$$u = J_0 + \mathcal{O}(J_0^3) \ ; \qquad v = \frac{J_0}{2} + \frac{5}{8} J_0^2 + \mathcal{O}(J_0^3) \ . \quad (22)$$

The resulting u, v can be inserted into the injection and ejection current forms, Eqs. (9) and (10) to obtain corresponding boundary rates. Such results, and corresponding level sublattice particle densities $U = u(1+u)$, $V = v(1+v)$ allow comparisons with results from steady state simulations.

Finally in this Subsection, still for the fully unpolarized case, we give results for the dividing line on the (α, β) phase diagram, between current independent of α and independent of β. By analogy with the standard 1D TASEP [3–7] this could possibly be the signature of a coexistence line, though we shall not investigate such a connection here.

The calculation involves the full range of possible site average occupations. Both forms of mean field theory outlined in Sec. II B 2 were used. That from the $C^\pm$ gives the line equation as

$$\alpha \, \frac{\left(1 - \frac{\alpha}{2}\right)}{\left(1 + \frac{\alpha}{2}\right)} = 2\beta \, \frac{(1-\beta)}{2-\beta} \ . \qquad (23)$$

A more complicated equation results from using the mean field theory from the $C^{\pm\prime}$, but in fact it turns out to make little quantitative difference.

5. *Effect of impurities on model (B)*

The mean field picture of spin-flipping processes is implicitly given in Sec. II B 2. Indeed, one can see that interchanging p_ℓ^+ and p_ℓ^- in Eqs. (7), (8) for the mean field current of bond ℓ, $\ell+1$ without impurity represents the spin flip and correct current with an impurity residing on site ℓ.

Recall that model (B) with unpolarized injection is unaffected by the (equivalent) flipping of plus and minus spins, so that case is covered by the results in Secs. II B 3 and II B 4, for chains and nanotubes respectively. We thence proceed to treat the nanotube with fully polarized injection (the corresponding case for the chain being trivial).

In the nanotube one has the branching and recombination of particle paths, leading to the statistical features already discussed for model (A) in Ref. 1. For model (B) the new effects, caused by the allowed conditional double occupancy, are most apparent at high densities of particles of both spins. This is evident for the unpolarized injection case in the low current high-density situation occurring, e.g., for $\alpha^+ = \alpha^- \gtrsim \beta^+ = \beta^-$, see the simulation results in Fig. 5. But in all cases, the profiles discussed in Sec. II B 4 are transformed by any specific configuration of impurities into successive sections

between the impurities in which the p_ℓ^+ and p_ℓ^- are interchanged. These give the qualitative features seen in the configuration-specific simulation results shown in Figs. 4 and 5.

Quantitative comparisons are possible using the density profiles for the pure nanotube for each successive section. Similarly, the mean field spin-up and spin-down particle currents J^+, J^- given previously are interchanged by the impurities, and their values can be compared with simulation results.

III. TASEP MODEL: NUMERICS

A. Introduction

For a structure with N_b bonds, an elementary time step consists of N_b sequential bond update attempts, each of these according to the following rules: (1) select a bond at random, say, bond ij, connecting sites i and j; (2) if the chosen bond has an occupied site to its left and an empty site to its right, then (3) move the particle across it, i.e., from i to j with probability (bond rate) p_{ij}. If an injection or ejection bond is chosen, step (2) is suitably modified to account for the particle reservoir (the corresponding bond rate being, respectively, α or β). Thus, in the course of one time step, some bonds may be selected more than once for examination and some may not be examined at all. This constitutes the *random-sequential update* procedure described in Ref. 13 for the 1D TASEP, which is the realization of the usual master equation in continuous time.

In order to account for particle spin, adaptations are needed. As in the original TASEP rules, we stick to the interpretation that a successful bond update attempt means the motion of a *single* particle across that bond. In model (B), for step (2) above one allows double occupancy if in agreement with Pauli's principle; furthermore, if site i itself is doubly occupied and site j is empty, then either particle may be moved from i to j with 50% probability. For step (3), with $\alpha^\uparrow$, $\alpha^\downarrow$ being the mutually exclusive, spin-dependent, particle injection rates ($\alpha \equiv \alpha^\uparrow + \alpha^\downarrow$), spins are independently chosen with probability $P^{\uparrow\,(\downarrow)} = \alpha^{\uparrow\,(\downarrow)}/\alpha$ for individual injection attempts. The case $\alpha^\uparrow = \alpha$ corresponding to a fully polarized injected current is of special interest. Also, the case of a fully depolarized incoming current, $\alpha^\uparrow = \alpha^\downarrow = \alpha/2$ will be considered below. With regard to ejection, if the rightmost site is singly occupied the particle is ejected with spin-independent probability β; for double occupation, the particle to be ejected (also with probability β) is chosen with 50% probability. The ejection procedures just delineated are consistent with our definition of an elementary bond update as involving crossing of the bond by at most a single particle; comments on the connection of this to actual experimental situations are made in Sec. IV. For the remainder of this paper, this amounts to replacing the ejection rates β^+, β^- introduced in Sec. II B 2 with a single, spin-independent, parameter β.

We evaluated steady-state currents, density profiles, and (normalized) spin polarizations. For the nanotube geometry, the steady-state current J is the time- and ensemble-averaged number of particles which enter the system per unit time, divided by the number N_w of parallel entry channels (to provide proper comparison with the strictly one-dimensional case). For each given realization of quenched randomness (collection of randomly-chosen locations of spin-flipping sites) we repeated the following procedure $N_{\rm sam} = 10$–100 times (each time with a distinct seed, i.e., producing $N_{\rm sam}$ independent samples of the stochastic update process): starting with an empty lattice, we kept injecting spin-up particles into the system's left edge, at a fixed injection rate α; after waiting for a suitable time until steady-state conditions set in, we would take $N_{\rm max} = 10^5$–10^6 successive realizations of stochastic update. As is well known [31, 32], the sample-to-sample RMS deviations for quantities estimated in this way are essentially independent of $N_{\rm sam}$ as long as $N_{\rm sam}$ is not too small, and vary as $N_{\rm max}^{-1/2}$. Furthermore, we considered N_q independent realizations of quenched disorder; for reasons to be explained below, both cases $N_q = 1$ (fixed-sample) and $N_q > 1$ (typically of order 100) turn out to be of interest. In contrast to the stochastic aspects just mentioned, disorder-associated sampling does not produce a distribution of results whose width shrinks with growing sample size: the pertinent distributions display a permanent spread, as will be exemplified in the following.

B. Chain without impurities: maximal current

In order to test the mean field theory of Sec. II B 3, in particular the predictions of Eqs. (16)–(18) concerning equal level profiles and the maximal current for model (B) on a chain with no impurities, we took unpolarized injection with $\alpha = \beta$ ranging from 0.6 to 1.0. We ran simulations with chain length $L = 41$, this length having proved sufficient to keep finite-size effects contained within the error bars associated with intrinsic stochastic fluctuations for $N_{\rm max} = 10^5$, and to provide approximately level sections to the profiles for $\alpha = \beta \lesssim 0.75$. For $\alpha = \beta = 1$ one gets the highest total current $J_m = 0.399(7)$, and a tan-like profile consistent with the maximal current phase [3–7]. The case $\alpha = \beta = 0.75$ has $J = 0.395(4)$. i.e., the same within quoted errors, and its profiles R, S range in the left half of the system by about ± 0.02 from the value ≈ 0.47 at the injection site. Thus, to a good approximation one can assume that both (α, β) pairs are within a maximal current phase analogous to the one exhibited by the standard TASEP. So the mean field prediction $J_m^- = J_m^+ = 0.243207\ldots$, and $R_m = 0.55671\ldots$ are of the order of 20% in excess of the numerical estimates.

On the other hand, the relationship Eq. (17), written in the form $J^+ = \alpha(1 - R)$, is verified by the numerical results within stochastic error, as should be expected be-

cause it requires no factorization approximation (unlike the other mean field relationships used).

C. Nanotube with impurities

We now turn to the nanotube geometry, in presence of impurities. In order to reduce non-essential fluctuations, we used a canonical ensemble to generate our impurity realizations. For a nanotube with N_s sites in all, and nominal impurity concentration x_i we would randomly draw m_i out of the N_s possible locations, m_i being the integer closest to $x_i\, N_s$. Consequently the effective concentration $x_i^{\rm eff}$ differs from x_i; however, even in the physically reasonable range $x_i \ll 1$ such discrepancy is very small for the (relatively large) systems used. In our simulations we generally took $x_i = 0.01$; for $N_w = 14$, $N_r = 20$ (a combination we used quite often, as seen below) one gets $m_i = 11$, giving $x_i^{\rm eff} = 11/1134 = 0.09700\ldots$

We started by fixing the external rates at $(\alpha, \beta) = (1/2, 1/2)$. For a nanotube with $N_w = 14$, $N_r = 20$ we examined the decay of the polarization $\mathcal{P}$ of a fully-polarized current injected at the system's left end, against position along the average flow direction. We collected data from $N_q = 10^6$ independent samples of impurity configurations, in order to produce smooth probability density curves at the right (exit) end, where an ejected particle would necessarily have gone through 81 sites. The results for models (A) and (B), as well as for the effective-medium (EM) approach described in Sec. II, are shown in Fig. 1. Averages and RMS dispersions are as follows: $\langle\mathcal{P}\rangle = 0.184(60)$, $0.177(48)$, $0.199(31)$ respectively for (A), (B), and EM. It is worth remarking that already with $N_q = 100$ the numerical estimates for both average polarizations and dispersions are very close to those just quoted: one gets $\langle\mathcal{P}\rangle = 0.181(60)$, $0.173(48)$ respectively for (A), (B), although the corresponding distributions are of course rather spiky and shapeless.

So, in this case: (i) whether single- or conditional-double occupancy is allowed has no clearly discernible effect on polarization decay; also (ii) the steady-state current through the system is $J = 0.3064(1)$ in (A), $0.307(1)$ in (B), identical within error bars (and in line with results for spinless systems with the same (α, β) [1]); furthermore, (iii) although the EM description predictably underestimates fluctuations, its result for the polarization distribution at the right end still falls well within the broader dispersion of both numerically-evaluated curves.

Next, we compare fixed-sample ($N_q = 1$) versus multiple-sample polarization results, still at $(\alpha, \beta) = (1/2, 1/2)$. For $N_q = 100$, Fig. 2 again shows the broad scatter associated with sampling over disorder configurations. By contrast, for the two examples corresponding to $N_q = 1$ (where the sharp downward steps correspond to x-values of the particular locations of spin-flipping sites in the respective disorder realization), the amount of spread (related exclusively to sampling over stochastic updates) is quite suppressed, as anticipated above.

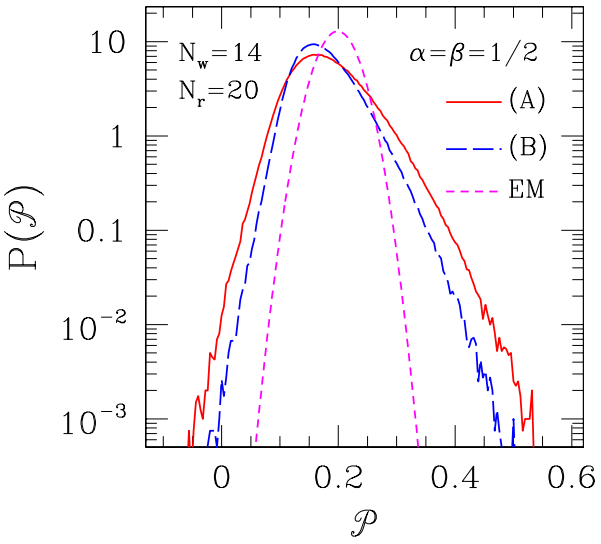

Figure 1. Log-linear plot of probability density function for polarization at the right end (exit) of a nanotube, for a current injected with $\mathcal{P}_{\rm in} = 1$ at its left end. Here $\alpha = \beta = 1/2$, $N_w = 14$, $N_r = 20$, $x_i = 0.01$. (A) and (B) refer, respectively, to models with single or conditional-double site occupation; in both cases, samples were taken over $N_q = 10^6$ distinct realizations of impuritiy configurations. EM refers to the effective-medium description given in Sec. II.

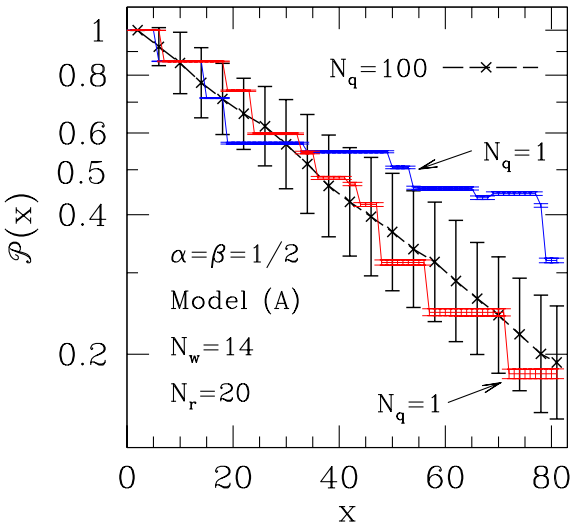

Figure 2. Log-linear plot of polarization against position x along average flow direction of a nanotube, for a current injected with $\mathcal{P}_{\rm in} = 1$ at its left end. Here $\alpha = \beta = 1/2$, $N_w = 14$, $N_r = 20$, $x_i = 0.01$. Each of the polarization profiles denoted $N_q = 1$ (blue and red) corresponds to a distinct, fixed, realization of the impurity distribution.

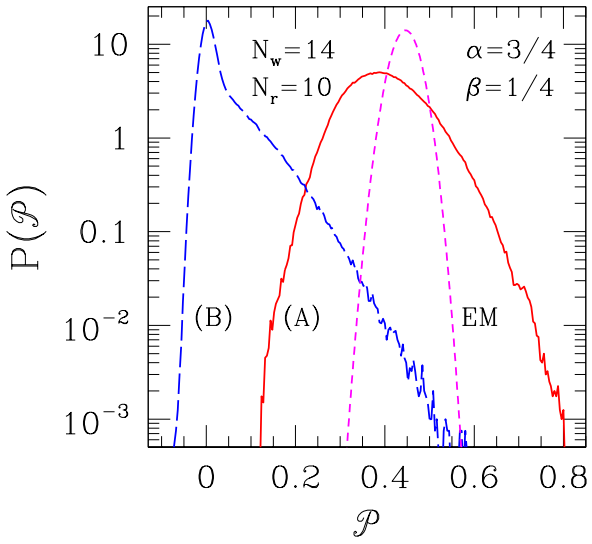

Figure 3. Log-linear plot of probability density function for polarization at the right end (exit) of a nanotube, for a current injected with $\mathcal{P}_{\rm in} = 1$ at its left end. Here $\alpha = 3/4$, $\beta = 1/4$, $N_w = 14$, $N_r = 10$, $x_i = 0.01$. (A) and (B) refer, respectively, to models with single or conditional-double site occupation; in both cases, samples were taken over $N_q = 10^6$ distinct realizations of impurity configurations. EM refers to the effective-medium description given in Sec. II.

It can be seen that the central estimates for the $N_q = 100$ curve are well aligned, suggesting a simple exponential dependence, $\mathcal{P}(x) \propto \exp(-x/x_0)$ against position. A fit gives $x_0 = 47.9(2)$. This is to be compared with $N_0 = 49.5$ from Eq. (3) with $x_i = 0.01$. Although the large scatter associated with each individual data point means that only limited significance can be attached to this result, it is remarkable that the sequence of average polarizations behaves so regularly.

Similar calculations for model (B) gave results very close to those displayed, for model (A), in Fig. 2.

Changing the external rates to $(\alpha, \beta) = (3/4, 1/4)$ produced drastically distinct results for polarization decay, especially regarding differences between models (A) and (B). This is seen in Fig. 3, where data for $N_w = 14$, $N_r = 10$ are shown. A shorter system than for $(\alpha, \beta) = (1/2, 1/2)$ was used in order to produce a nontrivial structure of the distribution for model (B); had we used $N_r = 20$ this would give essentially a delta function centered at zero, on the scale of Fig. 3 (see the corresponding entry in Table I below). So, while the probability density function for exiting polarization in model (A) compares to the EM prediction in a similar manner to the case $(\alpha, \beta) = (1/2, 1/2)$, allowing double occupancy here has a strong polarization-curbing effect.

We then varied α and β, probing selected points in the parameter space. Our results are displayed in Table I.

The main feature evinced is a clear separation into

Table I. For systems with $x_i = 0.01$, $N_w = 14$, $N_r = 20$, and α, β as specified, $J(A)$, $J(B, X)$ are steady-state currents for: model (A) with initial polarization $\mathcal{P}_{\rm in} = 1$, and model (B) with $\mathcal{P}_{\rm in} = X$, $X = 0$ or 1. $\mathcal{P}_{\rm ex}$ denotes polarization at the system's exit. All from numerical simulations with $N_{\rm max} = 10^6$, $N_q = 100$. See text for further explanation of groups (I), (II), and (III).

α, β	$J(A)$	$J(B,1)$	$J(B,0)$	$\mathcal{P}_{\rm ex}(A)$	$\mathcal{P}_{\rm ex}(B,1)$
			(I)		
1/4, 1/4	0.1963(1)	0.1963(1)	0.2184(1)	0.179(56)	0.184(54)
1/4, 1/2	0.1963(1)	0.1963(1)	0.2184(1)	0.178(54)	0.176(50)
1/4, 3/4	0.1963(1)	0.1963(1)	0.2184(1)	0.188(64)	0.181(52)
1/2, 1/2	0.3064(1)	0.307(1)	0.3755(1)	0.183(53)	0.177(47)
1/2, 3/4	0.3064(1)	0.307(1)	0.3755(1)	0.179(61)	0.176(44)
			(II)		
1/2, 1/4	0.2133(1)	0.2457(1)	0.2457(1)	0.187(69)	0.001(4)
3/4, 1/4	0.2133(1)	0.2457(1)	0.2456(1)	0.190(68)	0.000(4)
			(III)		
3/4, 1/2	0.3336(1)	0.355(5)	0.4561(2)	0.184(56)	0.168(39)
3/4, 3/4	0.34817(4)	0.355(5)	0.4771(1)	0.177(46)	0.177(46)
1, 1	0.35069(3)	0.369(9)	0.5314(1)	0.188(64)	0.168(44)

three distinct patterns of behavior. For group (I), one has (with the definitions given in the caption to Table I): $J(A)$ depending only on α, $J(A) = J(B,1) < J(B,0)$, and (within error bars) $\mathcal{P}_{\rm ex}(A) = \mathcal{P}_{\rm ex}(B,1)$. For group (II) $J(A)$ depends only on β, $J(A) < J(B,1) = J(B,0)$; $\mathcal{P}_{\rm ex}(B,1) = 0$ while $\mathcal{P}_{\rm ex}(A) > 0$. For group (III) one has $J(A) < J(B,1) < J(B,0)$ and $\mathcal{P}_{\rm ex} > 0$ for both (A) and $(B,1)$. Note that for all cases with $\mathcal{P}_{\rm ex} > 0$ the prediction of the effective-medium approach of Sec. II, namely that $\mathcal{P}_{\rm ex}$ does not depend on α, β, seems to be qualitatively and, to a reasonable extent quantitatively, fulfilled.

As expected from the mean field theory in Sec. II B one can draw a correspondence between group (I) and the low-current, low-density phase of 1D TASEP [3, 6] where J is determined singly by α for $\alpha < \beta$, $\alpha < 1/2$. Similarly, group (II) has its analogue in the low-current, high density phase $\alpha > \beta$, $\beta < 1/2$ of the 1D case where J depends only on β. Finally, group (III) seems to be akin to the 1D maximal-current phase at $\alpha, \beta > 1/2$, although this remark will have to be qualified, as seen below. A phase with maximal-current features has been found for large α, β in earlier studies of TASEP on honeycomb lattices, see Fig. 7 of Ref. 1.

It is to be noticed that the fractional standard deviations of currents in Table I are, in general, of similar magnitude in models (A) and (B), and much smaller than those of exit polarizations (when the latter are nonzero), even though both quantities result from averaging over quenched disorder configurations. Although such feature is certainly expected for model (A) where current and polarization aspects are fully decoupled, it is not obviously forthcoming in model (B). To understand this it

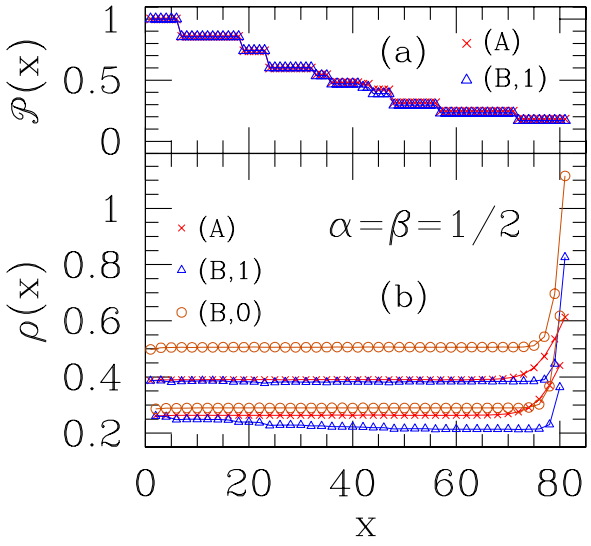

Figure 4. (a) Polarizations $\mathcal{P}(x)$ and (b) full densities $\rho(x)$ (spin-up plus spin-down) against position x along average flow direction of a nanotube with $N_w = 14$, $N_r = 20$, $x_i = 0.01$, $(\alpha, \beta) = (1/2, 1/2)$ for a current injected with $\mathcal{P}_{\rm in} = 1$ [A, $(B,1)$] or $\mathcal{P}_{\rm in} = 0$ [$(B,0)$] at its left end. In all cases, the same fixed impurity realization has been used ($N_q = 1$); for each of models (A) and (B), the two sequences of distinct sublattice densities [1, 2] are plotted separately for ease of visualization.

must be kept in mind that, for each fixed disorder configuration, current evaluation involves extensive stochastic sampling of allowed particle motions. Averaging over the latter ensemble has the effect that, in model (B) as well as (A), the influence of spin-flipping impurities on the system-wide current shows up only through their overall concentration (as opposed to depending on their specific locations).

Further insight into the contrasting behavior of models (A) and (B) in groups (I) and (II) can be gained by studying the respective steady-state density profiles. In order to have an unbiased view of the stochastic effects involved in establishing and maintaining the stationary regime, we suppressed fluctuations related to sampling over quenched disorder by using the *same* fixed impurity configuration ($N_q = 1$) in all cases depicted in the following Figs. 4 and 5.

For the low-density case $(\alpha, \beta) = (1/2, 1/2)$, the density profiles are very similar for both models, while the fixed-sample polarization results are nearly identical on the scale of Fig. 5. This confirms that the additional degree of freedom provided by allowing double occupation plays only a minor role here.

Furthermore, we recall that domain-wall theory predicts, and it has been numerically verified [33], that for ordinary TASEP with spinless particles on staggered chains the difference between steady-state sublattice density profiles is constant, i.e., $x-$independent. This feature turns out to hold in the case of Fig. 4 for model (A) and, to a very good extent, for model (B) with $\mathcal{P}_{\rm in} = 0$, but not so for (B) with $\mathcal{P}_{\rm in} = 1$. Such agreement would be expected for model (A) where spatial and spin degrees of freedom are effectively decoupled, because it is known that (i) domain-wall and mean-field theory give identical predictions for steady-state properties of TASEP on (homogeneous or staggered) 1D chains [33]; and (ii) the mean field description of TASEP on a hexagonal lattice with uniform bond rates coincides with that of a chain with alternating bond rates $p_1 = 1$, $p_2 = 1/2$ [1, 2]. On the other hand, the fact that the constant-difference effect carries across to model (B) with $\mathcal{P}_{\rm in} = 0$, but not if $\mathcal{P}_{\rm in} = 1$, indicates that the former behaves throughout the system similarly to the flow of two immiscible fluid species with equal local densities. For the latter, on average the spin-flipping sites provide transformation of the spin-up "species" onto the spin-down one along the system, until polarization finally approaches zero, and the sublattice density differences approach a constant value. So the effects of such "species transmutation" are not included in the mean field approach which predicts constant density profile differences.

We have verified that the "immiscible species" picture is only semi-quantitatively correct, on account of the long-range density correlations known to exist generally in the TASEP. Indeed, the injection and ejection rules described above suggest that, as far as densities are concerned one could approximate the flow of an incident current with $\mathcal{P}_{\rm in} = 0$ at rates α, β in model (B) as two separate copies of the flow of a spinless fluid at rates $\alpha/2$, β in model (A). However, for the system described in Fig. 4, the nearly constant single-spin densities for $5 \lesssim x \lesssim 70$ are $\rho_1 \approx 0.253$, $\rho_2 \approx 0.145$ with half-current $J/2 \approx 0.1878$ [from Table I] in (B,0) with $(\alpha, \beta) = (1/2, 1/2)$, while in model (A) with $(\alpha, \beta) = (1/4, 1/2)$ total particle densities are $\rho_1 \approx 0.215$, $\rho_2 \approx 0.127$ (not shown in the Figure) with $J = 0.1963(1)$ [from Table I].

In the high-density case $(\alpha, \beta) = (3/4, 1/4)$ depicted in Fig. 5, double-occupancy is paramount for the steady-state profile configurations, especially on the system's right half. The fact that the current is the same in model (B), both for initial polarization equal to one or zero (see Table I), confirms that the low-β bottleneck on the right plays the dominant role in establishing stationary flow.

Regarding the above considerations of the "immiscible species" picture for the flow with $\mathcal{P}_{\rm in} = 0$, one sees in Fig. 5 that the spatial extent $x \gtrsim 35$ of the region where $\mathcal{P}(x)$ has essentially vanished is slightly longer than that, $x \gtrsim 45$, where the profiles coincide for $\mathcal{P}_{\rm in} = 0$ and 1. So, density-wise the case (B,1) crosses over from a behavior like that of (A) , up to $x \lesssim 20$, towards that of (B,0) albeit with a "healing length" corresponding to $35 \lesssim x \lesssim 45$ along which, although $\mathcal{P} = 0$ already, the local densities have not fully converged to the same values as for (B,0).

In Fig. 6 we show polarization against position (averaged over quenched disorder realizations) for model (B)

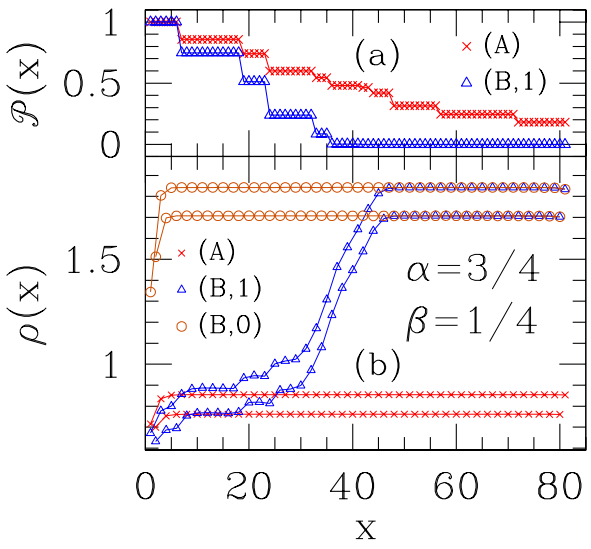

Figure 5. (a) Polarizations $\mathcal{P}(x)$ and (b) full densities $\rho(x)$ (spin-up plus spin-down) against position x along average flow direction of a nanotube with $N_w = 14$, $N_r = 20$, $x_i = 0.01$, $(\alpha, \beta) = (3/4, 1/4)$ for a current injected with $\mathcal{P}_{\rm in} = 1$ [A, $(B,1)$] or $\mathcal{P}_{\rm in} = 0$ [$(B,0)$] at its left end. In all cases, the same fixed impurity realization has been used ($N_q = 1$); for each of models (A) and (B), the two sequences of distinct sublattice densities [1, 2] are plotted separately for ease of visualization.

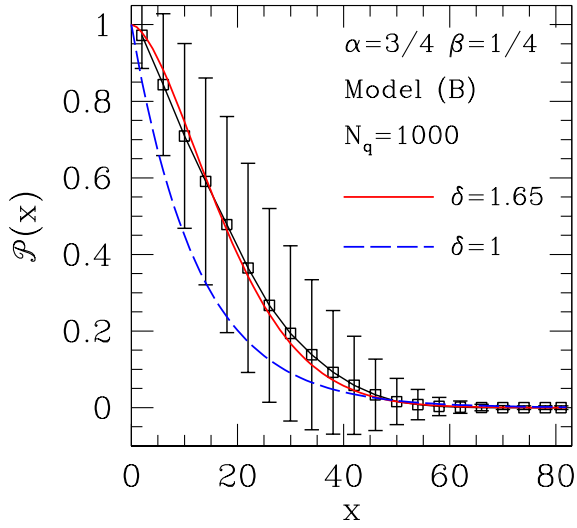

Figure 6. Polarization against position x along average flow direction of a nanotube, for a current injected with $\mathcal{P}_{\rm in} = 1$ at its left end. Here $\alpha = 3/4$,$\beta = 1/4$, $N_w = 14$, $N_r = 20$, $x_i = 0.01$. Average over $N_q = 1000$ distinct realizations of the impurity distribution. The curves correspond to fits of central estimates to a form $\mathcal{P}(x) = \exp\left[-(x/x_0)^\delta\right]$ (see text).

with $(\alpha, \beta) = (3/4, 1/4)$. It is clear that, contrary to the case depicted in Fig. 2, fitting a pure exponential form to the sequence of central estimates (blue, long-dashed curve in Fig. 6) gives unsatisfactory results. However, considering a generalized exponential function $\mathcal{P}(x) = \exp\left[-(x/x_0)^\delta\right]$ gives a much closer fit with $\delta = 1.65(4)$; see the full red line in Fig. 6.

We investigated the effects of system size on the results exhibited so far. In agreement with previous studies for spinless sytems [1, 2] the dependence of overall currents and average densities on transverse (N_w) and longitudinal (N_r) dimensions is rather weak. Regarding polarization-specific features, we checked the characteristic decay lengths x_0, both in the low- and high-density phases, as well as the phenomenological parameter δ for the latter case. As expected, the N_w dependence is residual. We found also that x_0 as well as δ (the latter, where pertinent) also exhibit only a weak N_r dependence. This is not obvious from the outset, especially for the high-density phase in model (B), given the influence of low β at the ejection sites on the buildup of double occupation backwards from there (see Figs. 5 and 6); in this case, for $N_r = 20$, 30, 40 one gets [keeping $\delta = 1.65$ fixed] $x_0 = 21.1(4)$, 23.8(7), and 25.7(9) respectively.

Next we examined the transition between the patterns of behavior characterizing groups (I) and (II) of Table I. Keeping $\alpha = 1/2$ fixed we varied β from 0.25, within the high-density (HD) phase, to 0.50, within the low-density (LD) one. Fig. 7 shows exit polarization $\mathcal{P}_{\rm ex}$ and steady-state current J. One sees that for $\beta \approx 0.32$ the current for (B,1) sharply turns from being equal to that of (B,0) to a constant value against increasing β, indicating an $\alpha-$dominated regime there, and eventually merging with $J(A)$ for $\beta \gtrsim 0.43$. Though the departure in behavior of $\mathcal{P}_{\rm ex}$ for (B,1) from the (B,0) pattern is not as clearly demarked as for J, it converges faster to that of (A), say by $\beta \approx 0.34$. We scanned the β axis also for different values of fixed α, namely 1/4, 3/4, and 1. In all cases we found the same qualitative picture as that given for $\alpha = 1/2$ in Fig. 7. The $\alpha-$ dependence of the β value for which the current for (B,1) becomes constant against varying β is given approximately by

$$\beta(\alpha) = 0.8\alpha - 0.4\alpha^2 \ . \qquad (24)$$

Going back to Table I and referring to Eq. (24), one sees that the (B,1) results for $(\alpha, \beta) = (3/4, 3/4)$ and $(3/4, 1/2)$ are both associated with the intermediate-behavior section analogous to the $0.32 \lesssim \beta \lesssim 0.43$ stretch in Fig. 7.

Corresponding analysis of numerical data for the unpolarized case (B,0) provides a test of the theoretical results obtained in Eq.(23), see Table II. One sees that the agreement between mean field theory and numerics is very good in this case.

In order to provide further checks of the mean field theoretical predictions from Sec. II B 4 we took $(\alpha, \beta) = (1/4, 1/4)$. These rates, as can be seen from Table I, correspond to a point deep in the low-current, low-density

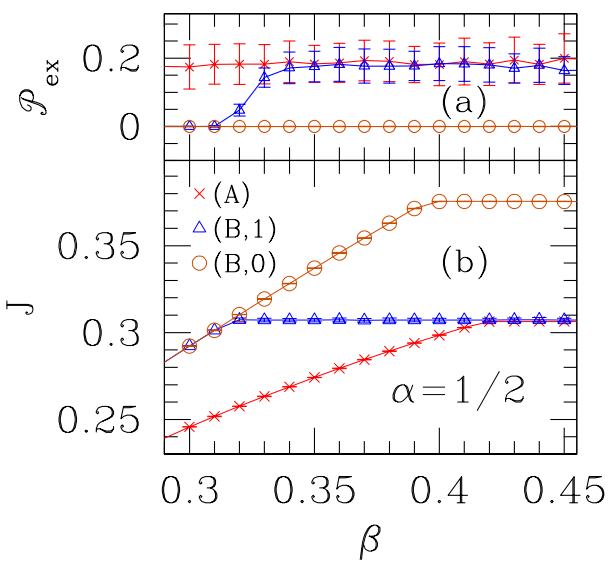

Figure 7. (a) Polarization at right end and (b) steady-state current J for a nanotube with $N_w = 14$, $N_r = 20$, $x_i = 0.01$, for a current injected with $\mathcal{P}_{\rm in} = 1$ [A, $(B,1)$] or $\mathcal{P}_{\rm in} = 0$ [$(B,0)$] at its left end, against ejection rate β. Injection rate $\alpha = 1/2$ (fixed). Averages over $N_q = 100$ distinct realizations of the impurity distribution.

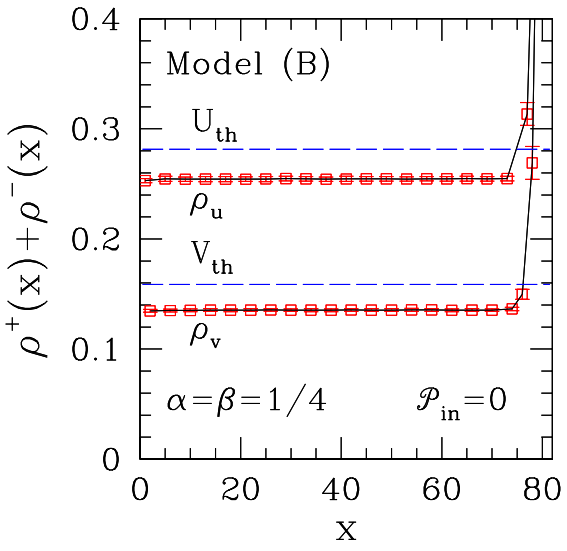

Figure 8. Points (ρ_u and ρ_v) show steady-state sublattice full (spin-up plus spin-down) densities against position along flow direction, for model (B) on a nanotube with $N_w = 14$, $N_r = 20$ at $(\alpha, \beta) = (1/4, 1/4)$. $\mathcal{P}_{\rm in} = 0$, so impurities are statistically irrelevant in establishing total current and density profiles. Horizontal dashed lines ($U_{\rm th}$ and $V_{\rm th}$) show mean field predictions derived from Eqs. (20)–(21). See text.

Table II. For model (B,0) and selected values of α, $\beta_{\rm th}$ are the values of β for which total current J becomes β-independent, as predicted by Eq.(23); $\beta_{\rm num}$ are numerically-obtained results (see, e.g., Fig. 7).

α	$\beta_{\rm th}$	$\beta_{\rm num}$
1/4	2/9	0.23(1)
1/2	2/5	0.40(1)
3/4	6/11	0.55(2)
1	2/3	0.65(2)

region of the phase diagram where both sublattice density profiles are expected to be level throughout the system (apart from an upturn close to the ejection end, see Fig. 4 for a less extreme example). Also, we took an unpolarized injected current, $\mathcal{P}_{\rm in} = 0$ so impurities would have no net effect. In such conditions one would expect the conditions expressed in Eqs. (20)–(21) to apply. Theoretical and simulational results are displayed, for both sublattices, in Fig. 8. The numerically-evaluated full (spin-up plus spin-down) densities for the level section of the profiles are: $\rho_u = 0.254(2)$, $\rho_v = 0.153(2)$, to be compared to the predictions from theory. The latter are found by plugging the full (numerically-evaluated) steady-state current $J = 0.2184(1)$ from Table I into the specific forms of Eqs. (7), (8) given by Eq. (21), and solving for $U \equiv u(1+u)$, $V \equiv v(1+v)$. One gets $U_{\rm th} = 0.2814(2)$, $V_{\rm th} = 0.1586(1)$, respectively 10% and 4% in excess of simulation results. Then inserting J and $U_{\rm th}$ into left- and right-hand sides of Eq. (9) gives $\alpha = 0.3039(4)$, different by $\sim 20\%$ from the actual value 1/4.

We have also checked how the characteristic decay length x_0 depends on impurity concentration. In this case we restricted ourselves to $(\alpha, \beta) = (1/2, 1/2)$, well within the portion of phase space for which polarization decay follows a simple exponential form. We considered $x_i = 0.003$, 0.005, 0.0075, and 0.01, all in the very low impurity-density regime. For model (B) with $\mathcal{P}_{\rm in} = 1$ we took systems of fixed width $N_w = 14$ and varying lengths in the range $20 \le N_r \le 120$. For fixed x_i the final estimates of x_0 took into account the dispersion among the results of the individual fits for each N_r. The sequence of the $\{x_0\}$ was adjusted to a power-law form, $x_0 \propto x_i^{-a}$, whence $a = 1.03(2)$. This agrees well with the result $a = 1.1(1)$ of Ref. 25.

We now illustrate how the interplay of double occupancy and spin-flipping impurities can result in an enhancement of the steady state current across the system. Taking model (B) with a fully polarized current injected at the left end ($\mathcal{P}_{\rm in} = 1$), we considered $\alpha = \beta = 1$. In this way the constraints imposed by boundary conditions are minimized, and the remaining impediments to particle flow are only those associated with exclusion according to Pauli's principle. In order to probe asymptotic trends, we allowed the impurity concentration to vary well beyond the physically reasonable regime $x_i \ll 1$. The results are shown for a system with $N_r = 14$, $N_r = 20$ in Fig. 9, together with an *ad hoc*

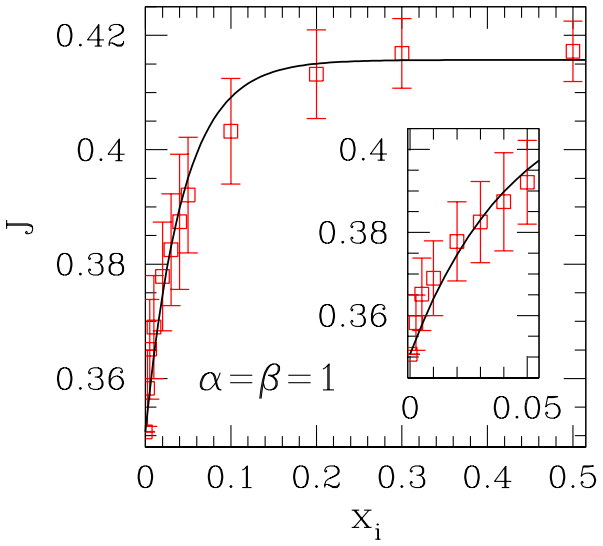

Figure 9. Steady-state current J as a function of impurity concentration x_i for model (B) at $(\alpha, \beta) = (1, 1)$ with a fully polarized current injected at the left end ($\mathcal{P}_{\rm in} = 1$). $N_w = 14$, $N_r = 20$. The full line is an *ad hoc* exponential fit to the data. The inset shows details of the main figure close to the vertical axis.

exponential fit to the data which gives the limiting current $J_{\rm lim} = 0.416(2)$. This is significantly higher than the value $J = 0.35069(3)$ for $x_i \equiv 0$, the latter coinciding with the (impurity-independent) current for model (A), see Table I. However, the impurity-induced current enhancement is not enough to equal the effect of injecting a fully depolarized beam for model (B), in which case the (also impurity-independent) corresponding value is $J = 0.5314(1)$, again from Table I. Overall, the resulting picture emphasizes the role played by Pauli's principle, in creating a bottleneck near the left end of the system for a polarized injected beam.

IV. DISCUSSION AND CONCLUSIONS

Model (B) introduced here bears a number of similarities with those generally known as "two-lane TASEP" models, in particular the implementation of Reichenbach *et al* [34, 35]. The latter authors consider strictly 1D systems with conditional double-occupancy rules obeying Pauli's principle. Their spin-flipping mechanism is purely stochastic, and it is shown that several nontrivial effects take place for specific (mesoscopic) ranges of its occurrence rate. We now outline relevant differences between our approach and theirs. In the present case, spin-flipping results from a combination of quenched and stochastic factors. These are respectively: fixed locations of spin-flipping sites (for each given realization of impurity distribution), and the fact that, for the honeycomb geometry, the paths effectively followed by particles are dynamically and randomly chosen within a highly degenerate sample space. These features stem naturally from those of the physical systems under consideration here, within the limitations of the classical model used for their description. For the same reason, we use distinct injection rates $\alpha^{\uparrow}$, $\alpha^{\downarrow}$ and a single, spin-independent ejection attempt rate β (in contrast with $\beta^{\uparrow}$, $\beta^{\downarrow}$ of Refs. 34, 35). This corresponds to an experimental arrangement where full control can be exerted, e.g., by spin filtering, on the polarization of an incoming electron beam, but the ejection mechanism at the system's end is a voltage-based, spin-independent one.

Model (A) discussed above turns out to be a convenient testing ground for the introduction of polarization features, and also to provide useful comparisons with model (B), especially as regards the relevance, or not, of double site occupancy in the latter. It can be seen, e.g., in Table I and Fig. 7, that the current in model (A) is a lower bound for that in the (B,1) implementation, i.e., model (B) with injected polarization $\mathcal{P}_{\rm in} = 1$ [the upper bound being given by (B,0)]. Accordingly, having $J(A) = J(B, 1)$ for a given (α, β) correlates well with having very similar, though not identical, density profiles; see Fig. 4. Conversely, $J(A) < J(B, 1)$ signals marked differences in such quantities, to the extent that double occupancy is very frequent along large sections of the system for the latter case, see Fig. 5.

As expected on general grounds, and from the mean field arguments in Sec. II B, both models (A) and (B) share with 1D TASEP the basic feature of exhibiting regions of the (α, β) plane where the overall current is solely determined either by injection (α) or ejection (β) rates, and which are associated respectively with low- or high-density profiles, see Figs. 4 and 5. For (B,1) the dividing line is given approximately by Eq. (24), to be compared with the corrresponding condition for 1D TASEP [3–9], namely $\alpha = \beta$. Furthermore, the discussion in the preceding paragraph indicates that for (B,1) the low- (high-) density phase is strongly connected with low (high) probabiliity of average occurrence of doubly-occupied sites.

One may propose a semi-quantitative correspondence of the TASEP rates (α, β) with physical parameters of electron transport on graphenelike structures. While the externally-imposed potential difference between injection and ejection points is the qualitative analogue of the directionality imposed by TASEP rules, its low or high intensity may be roughly mapped onto combinations of (α, β) which favor low or high currents, respectively. Additionally, the chemical potential difference $\Delta\mu_{L,R}$ between the graphenelike structure and leads on left and right is expected to be akin to α and β, respectively. Since usually one has $\Delta\mu_L = \Delta\mu_R$ [36], this would mean that experimental setups correspond to $\alpha = \beta$. In this case the results found here, especially the shape of the dividing line given by Eq. (24) and consequent implications, would indicate that double occupancy does not play a quantitatively significant role in electronic trans-

port on graphenelike structures.

ACKNOWLEDGMENTS

S.L.A.d.Q. thanks Belita Koiller for suggesting the problem, M.A.G. Cunha for clever insights during the early stage of calculations, A.R. Rocha for interesting discussions and for pointing out relevant references, and the Rudolf Peierls Centre for Theoretical Physics, Oxford, for hospitality during his visit. The research of S.L.A.d.Q. is supported by the Brazilian agencies Conselho Nacional de Desenvolvimento Científico e Tecnológico (Grant No. 303891/2013-0) and Fundação de Amparo à Pesquisa do Estado do Rio de Janeiro (Grants Nos. E-26/102.760/2012, E-26/110.734/2012, and E-26/102.348/2013).

[1] R. B. Stinchcombe, S. L. A. de Queiroz, M. A. G. Cunha, and Belita Koiller, Phys. Rev. E**88**, 042133 (2013).
[2] R. B. Stinchcombe and S. L. A. de Queiroz, Phys. Rev. E**91**, 052102 (2015).
[3] B. Derrida, Phys. Rep. **301**, 65 (1998).
[4] G. M. Schütz, in *Phase Transitions and Critical Phenomena*, edited by C. Domb and J. L. Lebowitz (Academic, New York, 2000), Vol. 19.
[5] B. Derrida, E. Domany, and D. Mukamel, J. Stat. Phys. **69**, 667 (1992).
[6] B. Derrida, M. R. Evans, V. Hakim, and V. Pasquier, J. Phys. A **26**, 1493 (1993).
[7] R. B. Stinchcombe, Adv. Phys. **50**, 431 (2001).
[8] R. A. Blythe and M. R. Evans, J. Phys. A **40**, R333 (2007).
[9] T. Chou, K. Mallick, and R. K. P. Zia, Rep. Prog. Phys. **74**, 116601 (2011).
[10] B. Schmittmann and R. K. P. Zia, in *Phase Transitions and Critical Phenomena*, edited by C. Domb and J. L. Lebowitz (Academic, New York, 1995), Vol. 17.
[11] R. Bundschuh, Phys. Rev. E**65**, 031911 (2002).
[12] T. Karzig and F. von Oppen, Phys. Rev. B**81**, 045317 (2010).
[13] N. Rajewsky, L. Santen, A. Schadschneider, and M. Schreckenberg, J. Stat. Phys. **92**, 151 (1998).
[14] S. L. A. de Queiroz and R. B. Stinchcombe, Phys. Rev. E**78**, 031106 (2008).
[15] J-C. Charlier, X. Blase, and S. Roche, Rev. Mod. Phys.**79**, 677 (2007); A. H. Castro Neto, F. Guinea, N. M. R. Peres, K. S. Novoselov, and A. K. Geim, *ibid.* **81**, 109 (2009).
[16] N. M. R. Peres, J. Phys. Condens. Matter **21**, 323201 (2009).
[17] E. R. Mucciolo and C. H. Lewenkopf, J. Phys. Condens. Matter **22**, 273201 (2010).
[18] I. Zutic, J. Fabian, and S. Das Sarma, Rev. Mod. Phys.**76**, 323 (2004).
[19] J. B. S. Mendes, O. Alves Santos, L. M. Meireles, R. G. Lacerda, L. H. Vilela-Leão, F. L. A. Machado, R. L. Rodríguez-Suárez, A. Azevedo, and S. M. Rezende, Phys. Rev. Lett.**115**, 226601 (2015).
[20] T. Ando, Phys. Rev. B**40**, 5325 (1989).
[21] S. N. Evangelou and T. Ziman, J. Phys. C **20**, L235 (1987).
[22] S. N. Evangelou, Phys. Rev. Lett.**75**, 2550 (1995).
[23] T. Ando, J. Phys. Soc. Jpn. **69**, 1757 (2000).
[24] Y. Asada, K. Slevin, and T. Ohtsuki, Phys. Rev. B**70**, 035115 (2004).
[25] S. L. A. de Queiroz, Phys. Rev. B**92**, 205116 (2015).
[26] S. Konschuh, M. Gmitra, and J. Fabian, Phys. Rev. B**82**, 245412 (2010).
[27] V. A. Rigo, T. B. Martins, A. J. R. da Silva, A. Fazzio, and R. H. Miwa, Phys. Rev. B**79**, 075435 (2009).
[28] J. Balakrishnan, G. K. W. Koon, M. Jaiswal, A. H. Castro Neto, and B. Özyilmaz, Nature Physics **9**, 284 (2013).
[29] A. Ferreira, T. G. Rappoport, M. A. Cazalilla, and A. H. Castro Neto, Phys. Rev. Lett.**112**, 066601 (2014).
[30] S. Irmer, T. Frank, S. Putz, M. Gmitra, D. Kochan, and J. Fabian, Phys. Rev. B**91**, 115141 (2015).
[31] R. B. Stinchcombe and S. L. A. de Queiroz, Phys. Rev. E**85**, 041111 (2012).
[32] S. L. A. de Queiroz and R. B. Stinchcombe, Phys. Rev. E**54**, 190 (1996).
[33] R. B. Stinchcombe and S. L. A. de Queiroz, Phys. Rev. E**94**, 012105 (2016).
[34] T. Reichenbach, T. Franosch, and E. Frey, Phys. Rev. Lett.**97**, 050603 (2006).
[35] T. Reichenbach, E. Frey, and T. Franosch, New J. Phys. **9**, 159 (2007).
[36] M. Politou, I. Asselberghs, I. Radu, T. Conard, O. Richard, C.-S.Lee, K. Martens, S. Sayan, C. Huyghebaert, Z. Tokei, S. De Gendt, and M. Heyns, Appl. Phys. Lett.**107**, 153104 (2015).